

Supplementary Information

Gold-Coated Silver Nanowires for long lifetime AFM-TERS probes

Han Wen,^a Tomoko Inose,^{*b} Kenji Hirai,^a Taiki Akashi,^a Shoji Sugioka,^a Jiangtao Li,^a Wannes Peeters,^c Eduard Fron,^c Beatrice Fortuni,^c Yoshihiko Nakata,^d Susana Rocha,^c Shuichi Toyouchi,^c Yasuhiko Fujita,^d and Hiroshi Uji-i^{*a, b, c}

a. Research Institute for Electronic Science (RIES) and Division of Information Science and Technology, Graduate School of Information Science and Technology, Hokkaido University, N20W10, Sapporo, Hokkaido 001-0020, Japan.

b. Institute for Integrated Cell-Material Science (WPI-iCeMS), Kyoto University, Yoshida, Sakyo-ku, Kyoto 606-8501, Japan.

c. Department of Chemistry, Division of Molecular Imaging and Photonics, KU Leuven, Celestijnenlaan 200F, B-3001 Leuven, Belgium.

d. Toray Research Center, Inc., Sonoyama 3-3-7, Otsu 520-8567, Shiga, Japan.

[*inose.tomoko.1v@kyoto-u.ac.jp](mailto:tinose.tomoko.1v@kyoto-u.ac.jp), hiroshi.ujii@es.hokudai.ac.jp, hiroshi.ujii@kuleuven.be

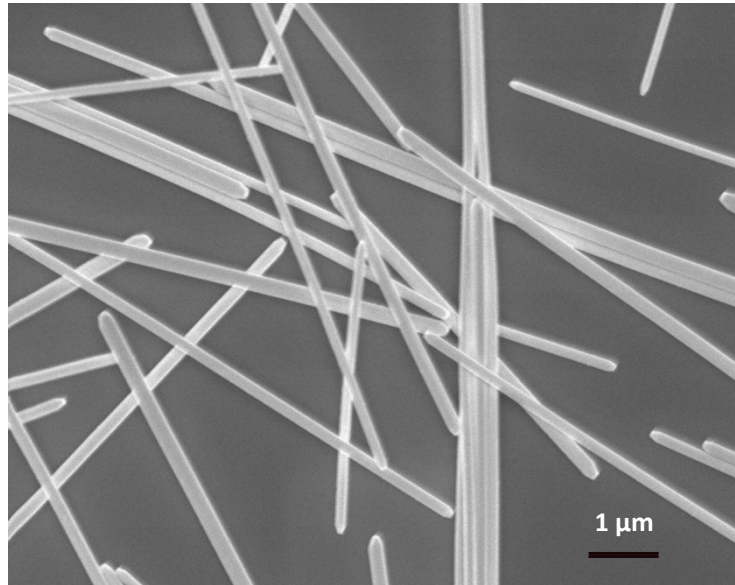


Fig. S1 SEM image of pristine AgNW

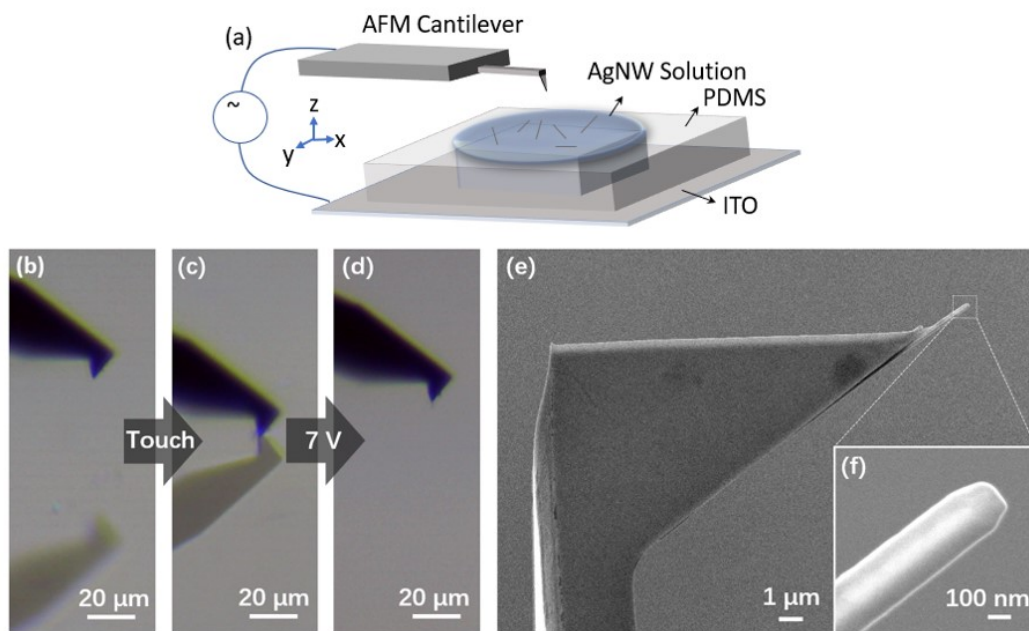


Fig. S2 (a) Schematic illustration of TERS probe fabrication; (b-d) optical transmission image of AgNW attachment: (b) before; (c) during; (d) after; (e-f) SEM image of TERS probe (using Ag@Au NW with n_{Au}/n_{Ag} equals to 3.85×10^{-6})

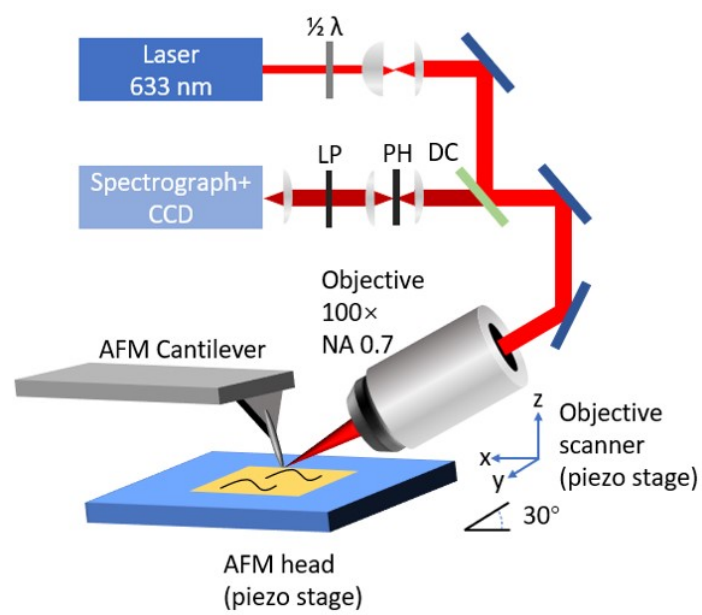


Fig. S3 Schematic illustration of AFM-TERS setup. (LP: long-path filter, PH: pin hole, DC: dichroic mirror, $\lambda/2$: half-wave plate, respectively)

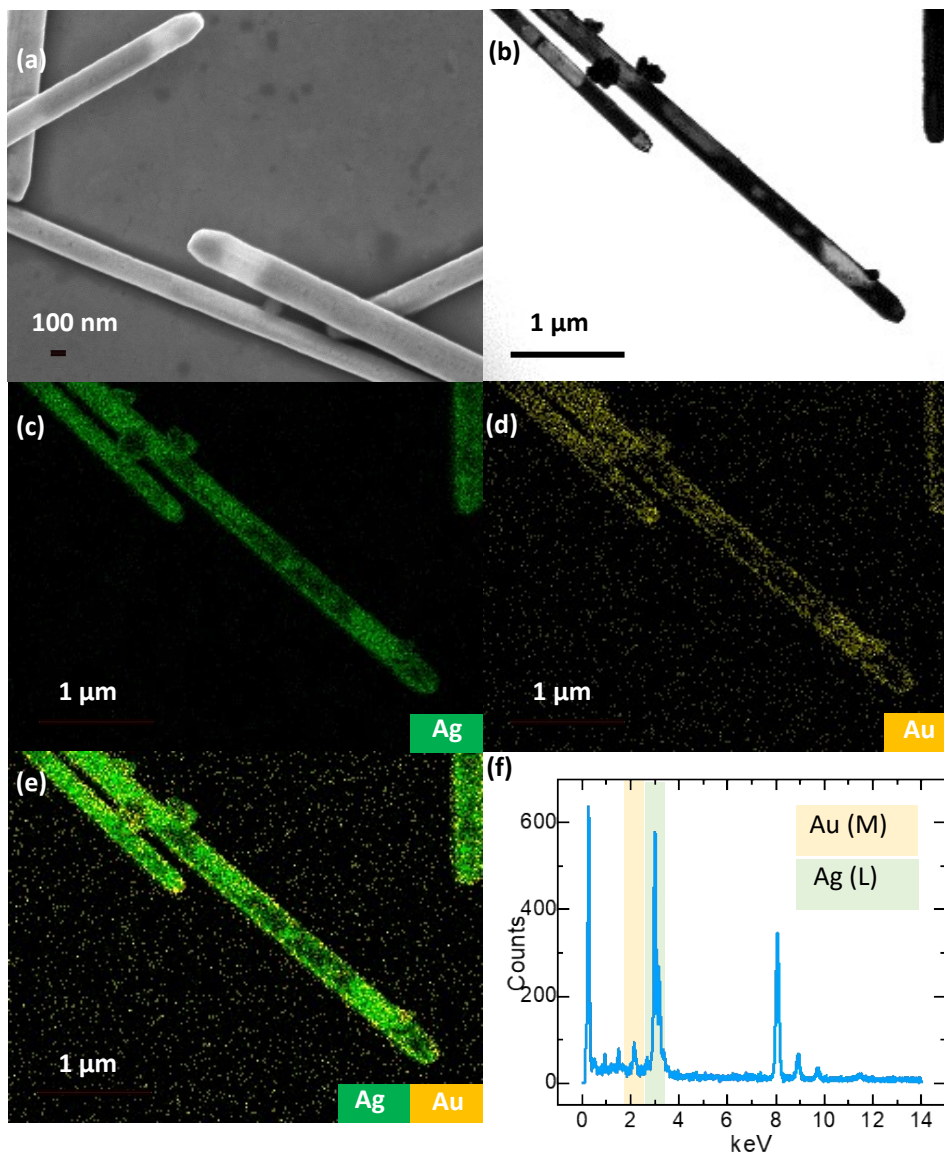


Fig. S4 Characterization of galvanic AgNW: (a) Low magnification SEM image; (b) Low magnification STEM image; (c) EDX mapping of Ag(L); (d) EDX mapping of Au (M); (e) EDX mapping of Ag (L) and Au (M); (f) EDX spectrum.

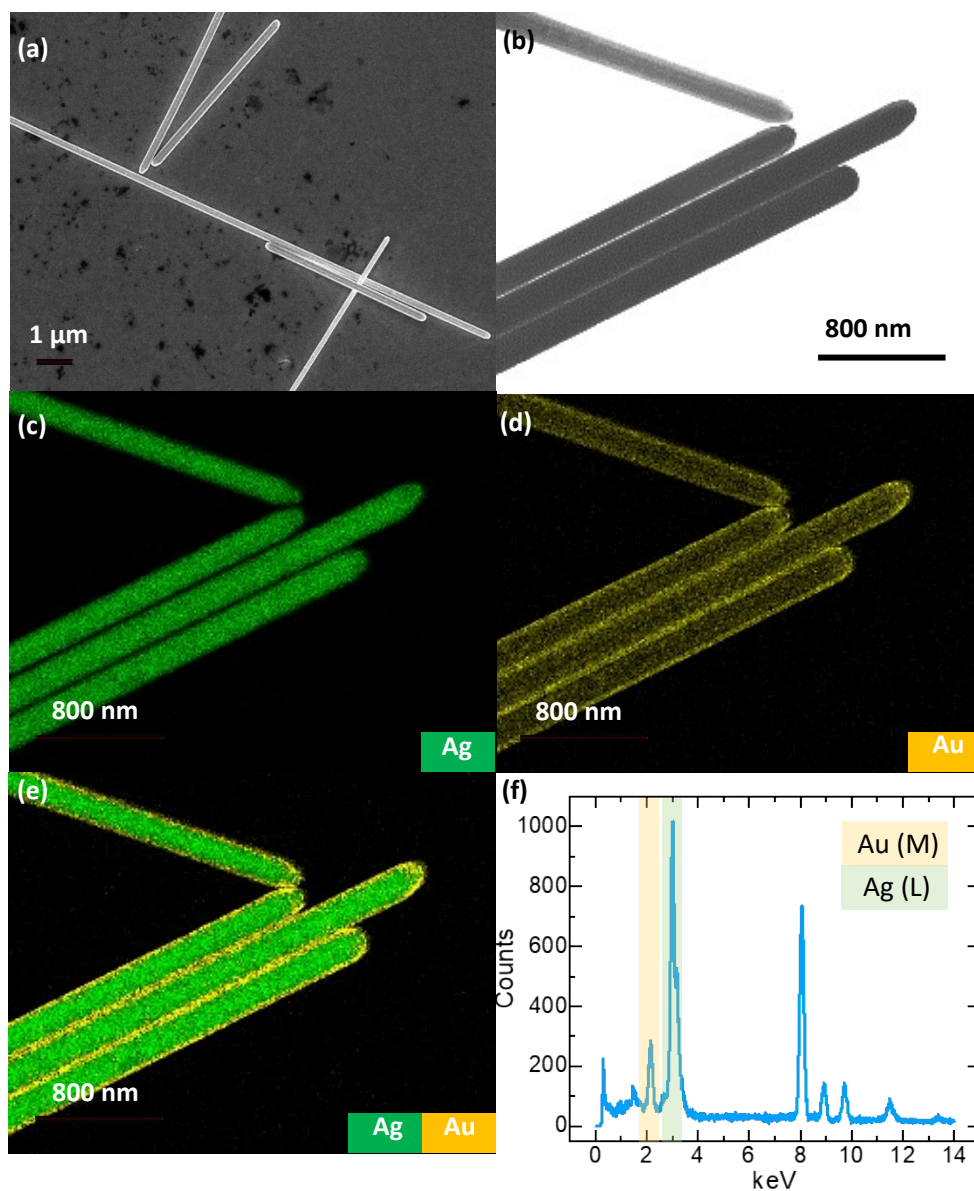


Fig. S5 Characterization of Ag@Au NW-H: (a) Low magnification SEM image; (b) Low magnification STEM image; (c) EDX mapping of Ag(L); (d) EDX mapping of Au (M); (e) EDX mapping of Ag (L) and Au (M); (f) EDX spectrum.

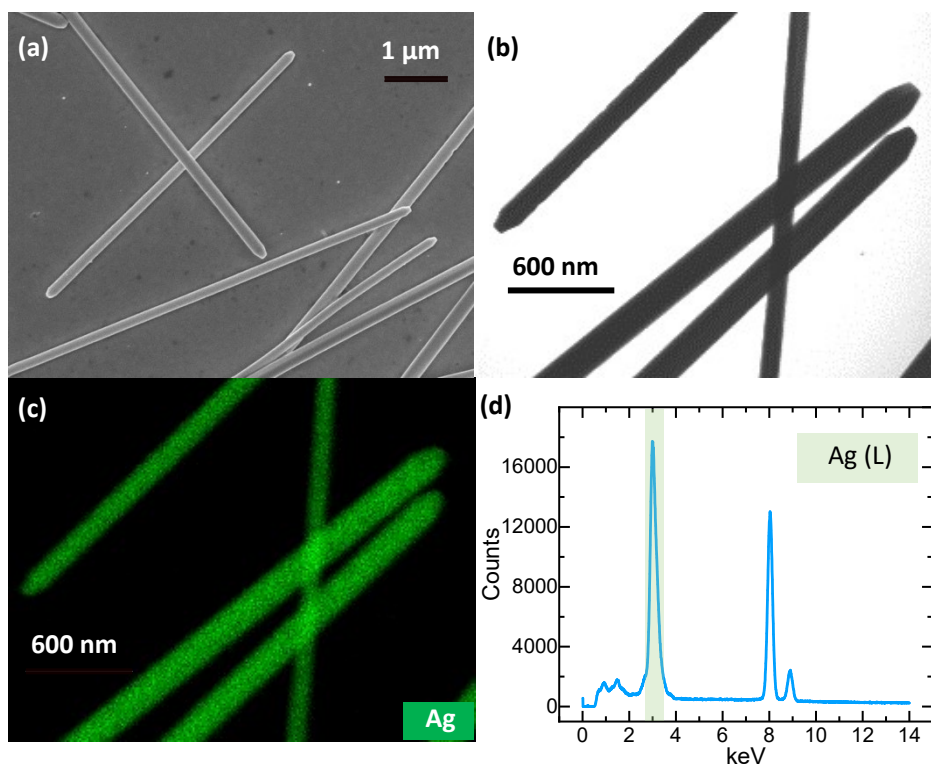


Fig. S6 Characterization of Ag@Au NW-L: (a) Low magnification SEM image; (b) Low magnification STEM image; (c) EDX mapping of Ag (L) (d) EDX spectrum.

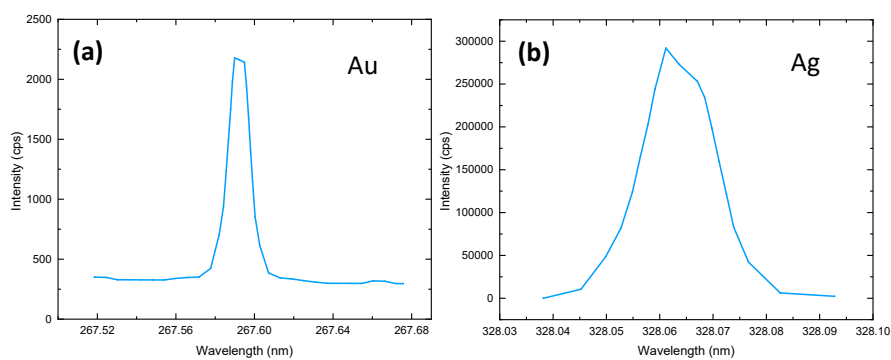


Fig. S7 ICP-OES of Ag@Au NW-H of (a): Au; (b): Ag

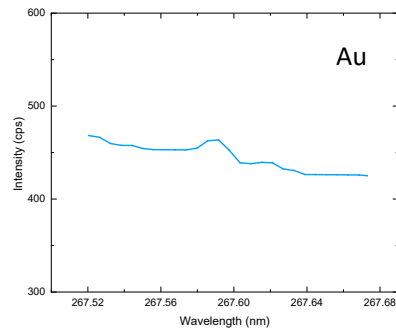


Fig. S8 ICP-OES of Ag@Au NW-L (Au)

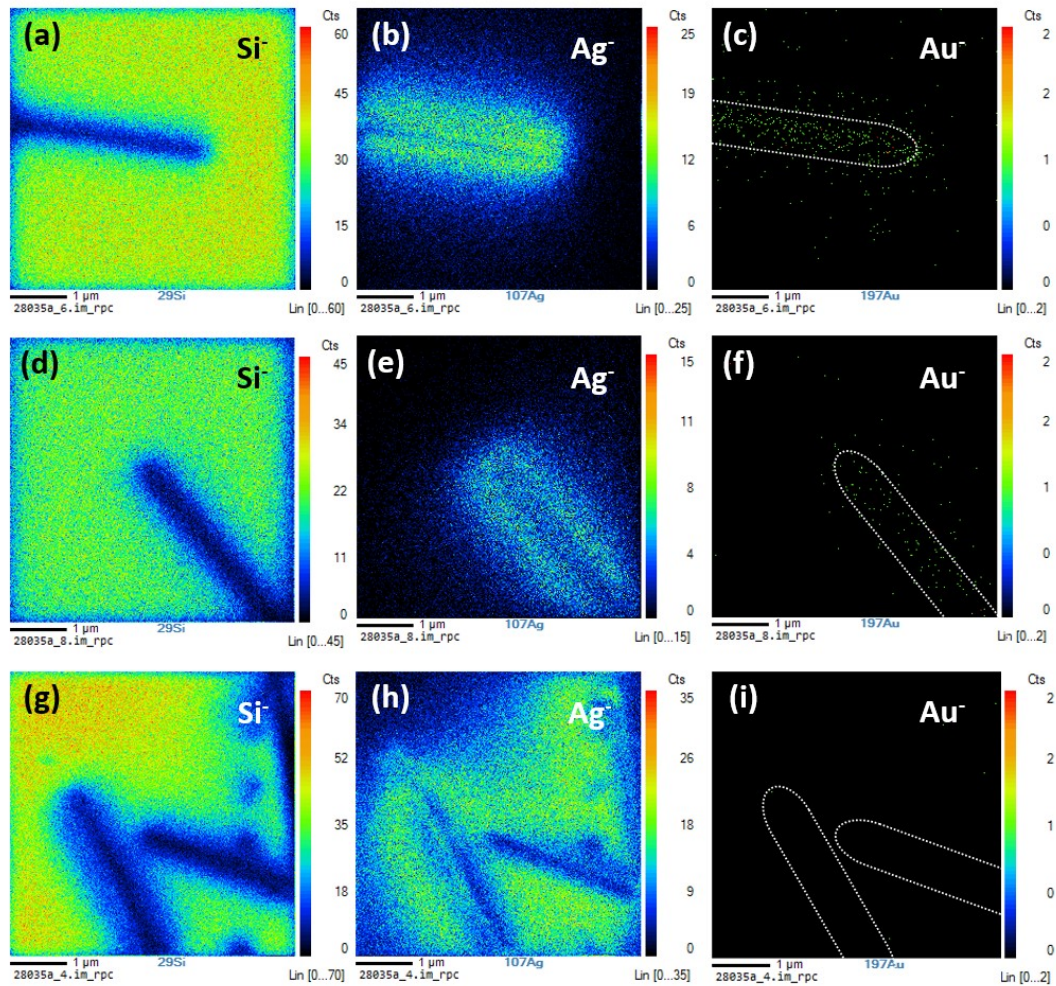


Fig. S9 NanoSIMS of Ag@Au NW-L and pristine AgNW: (a-c) NanoSIMS mapping of Si, Ag and Au of Ag@Au NW-L 1; (d-f) NanoSIMS mapping of Si, Ag and Au of Ag@Au NW-L 2; (g-i) NanoSIMS mapping of Si, Ag and Au of two pristine AgNWs.

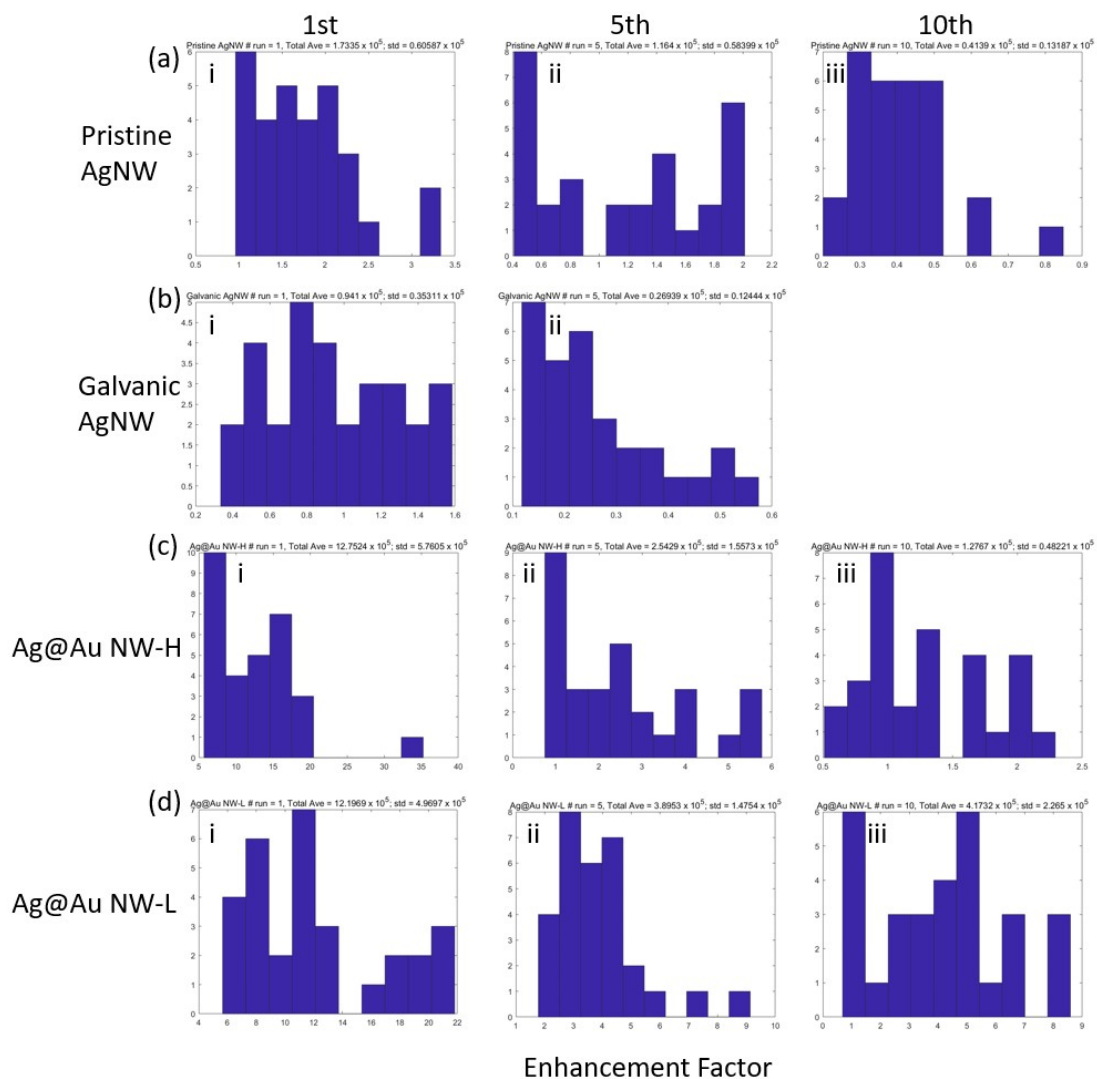


Fig. S10 Histogram of EF shown in figure 4: (a) pristine AgNW; (b) Galvanic AgNW; (c) Ag@Au NW-H; (d) Ag@Au NW-L. In each figure: i, ii, and iii: histogram of EF of 1st, 5th and 10th mappings respectively.

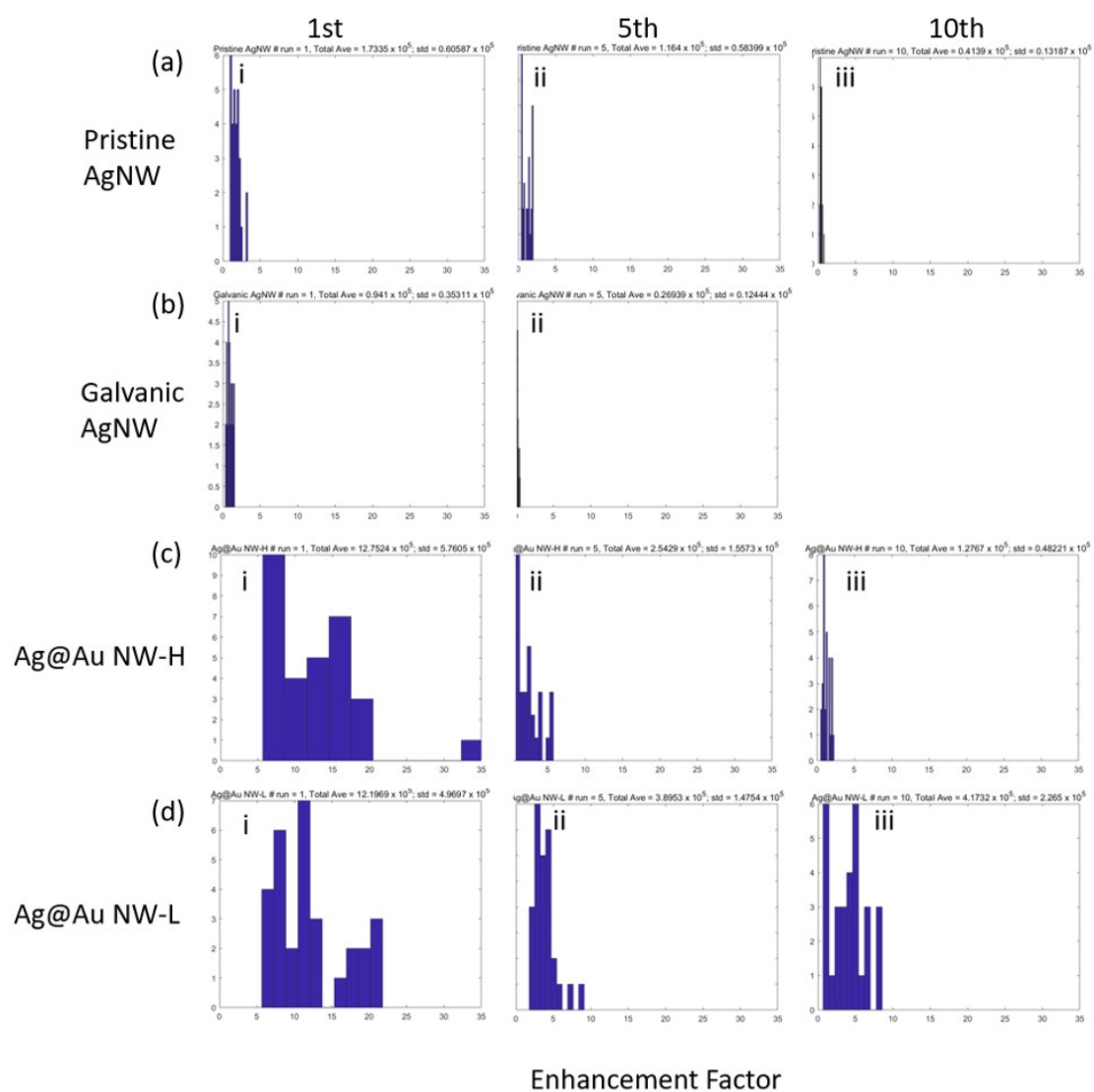


Fig. S11 Re-plot of Histogram of EF shown in figure S10 with the same range of x axis: (a) pristine AgNW; (b) Galvanic AgNW; (c) Ag@Au NW-H; (d) Ag@Au NW-L. In each figure: i, ii, and iii: histogram of EF of 1st, 5th and 10th mappings respectively.

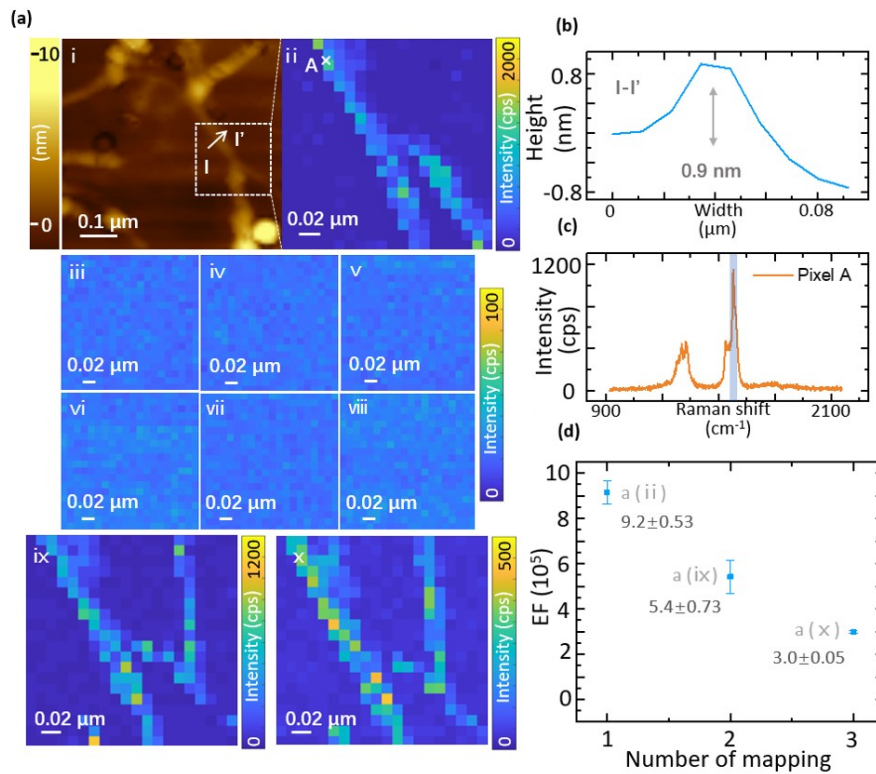


Fig. S12 Study of the effect of laser to EF using Ag@Au NW-H: (a) AFM image and TERS mapping: i: AFM image; ii 1st mapping under laser illumination; iii-viii: mappings without laser; ix: 2nd mapping with laser (8th mapping in total); x: 3rd mapping with laser (9th mapping in total); (b) line profile of CNT in (a)-i; (c) Raman spectrum of pixel A in ii; (d) EF of mappings with laser

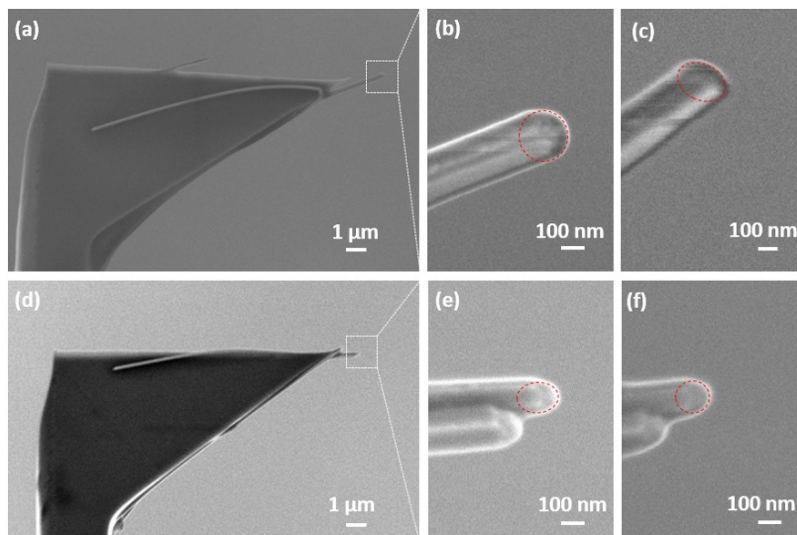


Fig. S13 Morphology change of Ag@Au NW-H: (a) Low magnification SEM image of probe 1; (b) high magnification SEM image before TERS measurement of probe 1; (c) high magnification SEM image after 10 mappings of TERS measurement of probe 1; (d) Low magnification SEM image of probe 2; (e) high magnification SEM image before TERS measurement of probe 2; (f) high magnification SEM image after 5 mappings of TERS measurement of probe 2.

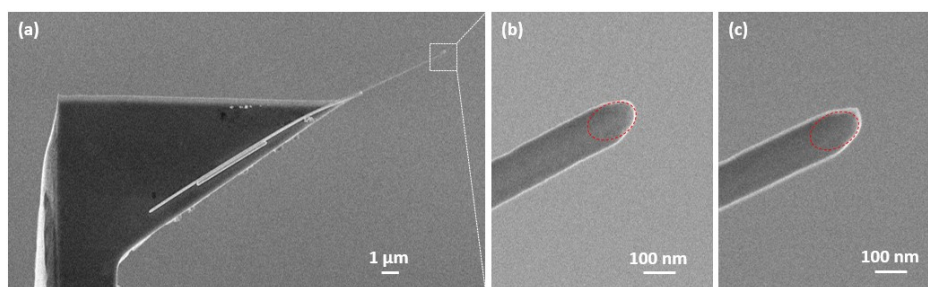


Fig. S14 Morphology change of Ag@Au NW-L: (a) Low magnification SEM image of probe; (b) high magnification SEM image before TERS measurement; (c) high magnification SEM image after 10 mappings of TERS.

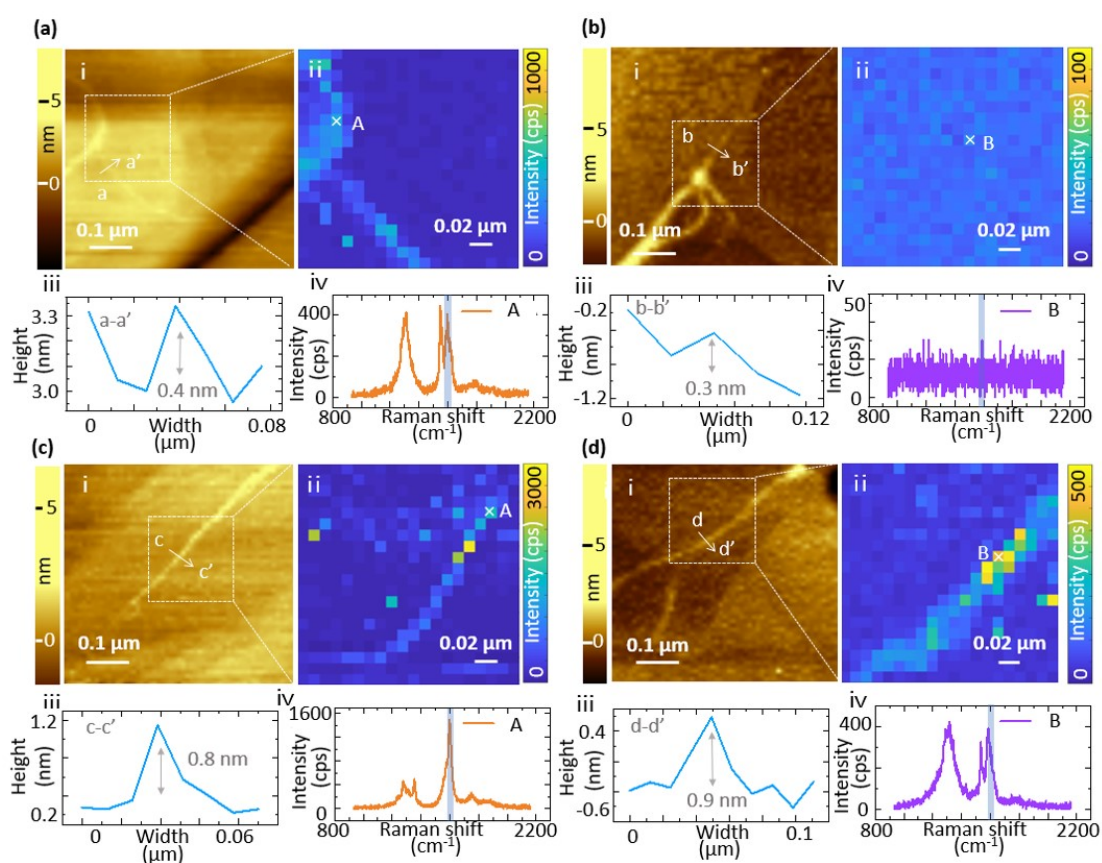


Fig. S15 Life time study of different TERS probes: (a) 1st mapping of pristine AgNW probe on the first day being prepared; (b) 1st mapping of the same pristine AgNW probe after one week (4th mapping in total); (c) 1st mapping of Ag@Au NW-L probe on the first day being prepared; (d) 1st mapping of the same Ag@Au NW-L probe after one week (4th mapping in total). In all subfigures, i refers to the AFM image; ii refers to the TERS mapping; iii refers to the line profile of the CNT in i; iv refers to the TERS spectra of the chosen pixel in ii. (Acquisition time was 0.4 s, accumulation once, 20×20 pixels (10 nm / pixel), Nf shift 80, laser power ~3.6 kW/cm², and the Raman intensity of G-band (cps) is selected to evaluate the TERS enhancement.)

Table S1. EF ($\times 10^5$) of three Ag@Au NW-L and three pristine AgNW probes at the first day (1~3) and after one week in air (4~6).

Mapping number		1st	2nd	3rd	4th	5th	6th
Ag@Au NW-L	P1	6.9	4.6	6.4	0.0	0.0	0.0
	P2	10.4	7.3	6.5	2.1	1.4	1.2
	P3	7.7	3.9	3.8	1.8	2.0	1.6
Pristine AgNW	P'1	3.3	1.1	0.9	0.18	0.18	0.17
	P'2	2.9	1.7	1.4	0.0	0.0	0.0
	P'3	1.7	1.0	0.7	0.0	0.0	0.0

Fitting of fig. 4

Equation S (1) to S (4) show the fitting results for pristine AgNW, Au-etched AgNW, Ag@Au NW-H and Ag@Au NW-L respectively. where EF refers to enhancement factor ($\times 10^5$) and n refers to TERS mapping numbers, m_i to number of mapping runs to reach $EF \sim 1/e$.

$$EF = \sum_{i=1}^{1 \text{ or } 2} \exp\left(-\frac{n}{m_i}\right)$$

$$EF = 2.1 \cdot e^{-\frac{n}{7.5}} \quad \text{S (1)}$$

$$EF = 1.2 \cdot e^{-\frac{n}{3}} \quad \text{S (2)}$$

$$EF = 18.9 \cdot e^{-\frac{n}{1.4}} + 4.2 \cdot e^{-\frac{n}{7.4}} \quad \text{S (3)}$$

$$EF = 31.7 \cdot e^{-\frac{n}{0.63}} + 6.1 \cdot e^{-\frac{n}{17.9}} \quad \text{S (4)}$$

Calculation of EF

The calculation method is shown in equations S (5) and S (6). C_{TERS} refers to TERS contrast, in which I_{TERS} and $I_{Far-Field}$ are the Raman intensity enhanced by near field and the intensity of normal far-field Raman. Here, the Raman intensity of G-band is picked as I_{TERS} since it is relatively stable and not affected by defect spots on the CNT, $I_{Far-Field}$ was measured under high laser power ($\sim 143 \text{ kW/cm}^2$) since it is almost impossible to obtain Raman signal with acceptable signal-to-noise ratio under same low laser power as TERS. Then, as the Raman signal is proportional to the laser power, the Raman signal is calculated by proportional compensating power difference. In equation (6), $A_{Far-Field}$ and $A_{Near-Field}$ refer to the area of far-field and near-field, respectively. The area of far-field can be easily calculated as the area of laser diffraction-limited focal spot by: diameter = $1.22 \lambda / NA$. However, the area of the near-field is hard to estimate, which is commonly calculated by numerical simulation. Nevertheless, the validity of simulation is limited since multiple assumptions are necessary. Here, the enhancing area is estimated by the TERS resolution, which is reported to be below 15 nm^1 , and in this experiment, 10 nm is regarded as the TERS resolution.

$$C_{TERS} = \frac{I_{TERS} - I_{Far-Field}}{I_{Far-Field}} \quad \text{S (5)}$$

$$EF = C_{TERS} \cdot \frac{A_{Far-Field}}{A_{Near-Field}} \quad \text{S (6)}$$

Reference

1. P. Walke, Y. Fujita, W. Peeters, S. Toyouchi, W. Frederickx, S. De Feyter and H. Uji-i, *Nanoscale*, 2018, 10, 7556-7565.